nature COMMUNICATIONS

ARTICLE

Received 18 Jul 2013 | Accepted 4 Sep 2013 | Published 24 Oct 2013

DOI: 10.1038/ncomms3558

Mitochondrial AtPAM16 is required for plant survival and the negative regulation of plant immunity

Yan Huang[1,2,*], Xuejin Chen[1,3,*], Yanan Liu[2,4], Charlotte Roth[5], Charles Copeland[1,2], Heather E. McFarlane[2], Shuai Huang[1,2], Volker Lipka[5], Marcel Wiermer[5] & Xin Li[1,2]

Proteins containing nucleotide-binding and leucine-rich repeat domains (NB-LRRs) serve as immune receptors in plants and animals. Negative regulation of immunity mediated by NB-LRR proteins is crucial, as their overactivation often leads to autoimmunity. Here we describe a new *mutant*, *snc1-enhancing* (*muse*) forward genetic screen, targeting unknown negative regulators of NB-LRR-mediated resistance in *Arabidopsis*. From the screen, we identify *MUSE5*, which is renamed as *AtPAM16* because it encodes the ortholog of yeast PAM16, part of the mitochondrial inner membrane protein import motor. Consistently, AtPAM16-GFP localizes to the mitochondrial inner membrane. *AtPAM16L* is a paralog of *AtPAM16*. Double mutant *Atpam16-1 Atpam16l* is lethal, indicating that AtPAM16 function is essential. Single mutant *Atpam16* plants exhibit a smaller size and enhanced resistance against virulent pathogens. They also display elevated reactive oxygen species (ROS) accumulation. Therefore, AtPAM16 seems to be involved in importing a negative regulator of plant immunity into mitochondria, thus protecting plants from over-accumulation of ROS and preventing autoimmunity.

[1] Michael Smith Laboratories, University of British Columbia, Vancouver, British Columbia V6T 1Z4, Canada. [2] Department of Botany, University of British Columbia, Vancouver, British Columbia V6T 1Z4, Canada. [3] College of Horticulture, Northwest A&F University, Yangling 712100, Shaanxi, China. [4] National Institute of Biological Sciences (NIBS), Beijing, China. [5] Department of Plant Cell Biology, Albrecht-von-Haller-Institute for Plant Sciences, Georg-August-University Göttingen, Julia-Lermontowa-Weg 3, 37077 Göttingen, Germany. * These authors contributed equally to this work. Correspondence and requests for materials should be addressed to X.L. (email: xinli@msl.ubc.ca).

Higher plants depend on their sophisticated immune systems to survive in nature. Two major types of immune receptors are responsible for microbial pathogen recognition and activation of downstream defence responses[1,2]. PAMPs (pathogen-associated molecular patterns; also known as microbe-associated molecular patterns) are recognized by plasma membrane-residing pattern recognition receptors (PRRs) to activate PAMP-triggered immunity (PTI). Successful pathogens are able to deliver specialized effectors (also termed Avirulence (Avr) proteins) into the host cell, which often perturb PTI to promote pathogen infection. On the other hand, plants have evolved *resistance* (*R*) genes to thwart pathogen infestation. These intracellular immune receptors recognize effectors to trigger a robust response termed effector-triggered immunity (ETI)[1,2], which often includes the accumulation of the plant hormone salicylic acid (SA), induction of *PATHOGENESIS-RELATED* (*PR*) genes, production of reactive oxygen species (ROS) and a localized cell death referred to as the hypersensitive response (HR). As ETI is often a much stronger response compared with PTI, R protein-mediated plant immunity has a central role in defeating adapted pathogen invasion. The majority of R proteins belong to the nucleotide-binding and leucine-rich repeat (NB-LRR) class[1], which can be further divided into two subclasses based on the presence of a Toll/Interleukin-1-receptor-like (TIR) or a coiled-coil (CC) domain at the N terminus[3]. Although many NB-LRR-encoding genes have been cloned in different plant species, it remains unclear how R proteins are activated.

Arabidopsis SNC1 (*SUPPRESSOR OF NPR1-1, CONSTITUTIVE 1*) encodes a TIR-type NB-LRR protein[4,5]. In the gain-of-function mutant allele *snc1*, a point mutation in the linker region between the NB and LRR results in a Glu-to-Lys change, which leads to the constitutive activation of defence responses without pathogen interaction. This mutant provides us with an ideal tool to study R protein-mediated immunity. To identify positive regulators of ETI, forward genetic suppressor screens were carried out to identify mutants that can suppress the autoimmune phenotypes of *snc1*. From these screens, we identified >10 *mos* (*modifier of snc1*) mutations, which revealed that RNA processing, protein modification, epigenetic control of gene expression and nucleocytoplasmic trafficking are important molecular events in R protein-mediated immunity[6]. Both MOS4 and MOS2 were identified as important positive regulators from the screens. MOS4 is a component of the nuclear spliceosome-associated MOS4-associated complex, which functions in regulating the proper splicing of *R* genes[7,8]. MOS2 contains one G-patch domain and two KOW motifs and is predicted to be involved in RNA processing pathways to regulate plant immunity[9]. The success of the MOS screen exemplifies the power of the unique *snc1* autoimmune model system to help dissect molecular events in ETI.

In the sophisticated signalling network of plant innate immunity, negative regulators are equally important for the regulation of defence responses as overactivation of plant defence would be detrimental for plant growth and development. Here we report our newly designed *snc1* enhancer screens aiming to identify negative regulators of R protein-mediated immunity. From this Mutant, *snc1*-enhancing (MUSE) genetic screen, we identified *MUSE5*, which encodes the ortholog of the *Saccharomyces cerevisiae* pre-sequence translocase-associated protein import motor (PAM) subunit PAM16 of the inner mitochondrial membrane. Although mitochondria have traditionally been believed to contribute positively to plant immunity through ROS generation, our study revealed an unexpected negative regulation on mitochondria's positive roles in plant defence. This regulation is probably achieved by a nuclear-encoded negative regulator of ROS generation, whose import into the mitochondrial matrix relies on AtPAM16.

Results

A modified *snc1* enhancer screen. Our previous MOS genetic screen identified positive regulators of *snc1*-mediated immunity. To explore negative regulators of R protein-mediated resistance, we performed two genetic screens to search for *snc1* enhancers in *mos4 snc1* and *mos2 snc1 npr1* backgrounds. Seeds of these two mutants, both containing a *pPR2::GUS* reporter gene, were mutagenized with ethyl methanesulfonate (EMS), and the M2 populations were screened for mutants that reverted to *snc1*-like morphology (dwarfed size and curly leaves). A secondary screen was then carried out to select only mutants with enhanced immunity. Expression of the defence marker gene *PR-2* was examined via GUS staining, and pathogen resistance was assessed by inoculating plants with the virulent oomycete *Hyaloperonospora arabidopsidis* (*H.a.*) Noco2. Over 20 heritable mutants were obtained from the screen, which were named *muse* (*mutant, snc1-enhancing*) mutants (Table 1). From the *muse* screens, we identified alleles of genes known to encode negative regulators of resistance, such as *bon1*, *cpr1*, *siz1*, and a gain-of-function *chs3-3d* allele[10] (Table 1). However, most of the *muse* mutants seem to carry mutations in novel genes that have not been studied in the past.

Characterization of *muse5-1 mos4 snc1*. The triple-mutant *muse5-1 mos4 snc1* was isolated from the mutagenized *mos4 snc1* population. This triple mutant reverts from the wild-type (WT)-like phenotype of *mos4 snc1* to a dwarf morphology similar to *snc1* (Fig. 1a). When the triple mutant was backcrossed with *mos4 snc1*, the F1 plants were all WT-like, indicating that *muse5-1* is recessive. To determine the defence phenotype of *muse5-1* in the *mos4 snc1* background, the expression of *PR-1* and *PR-2* was examined by RT–PCR. As shown in Fig. 1b, the expression of *PR-1* and *PR-2* was increased by *muse5-1* in *mos4 snc1* but not as strongly as

Table 1 | *snc1-enhancing* mutants identified from *mos snc1* backgrounds.

muse #	Lab code	Genetic background	Mutation
1	31-1	*mos4 snc1*	—
	9-1	*mos4 snc1*	—
	37-1	*mos4 snc1*	—
	15-2	*mos4 snc1*	—
	98-1	*mos4 snc1*	—
2	81-1	*mos4 snc1*	—
3	48-1	*mos4 snc1*	—
4	3-1	*mos4 snc1*	—
5	57-1	*mos4 snc1*	Current report
6	39-1	*mos4 snc1*	—
7	92-1	*mos4 snc1*	—
	LK83	*mos2 snc1 npr1*	—
8	471	*mos2 snc1 npr1*	—
9	10-2	*mos4 snc1*	—
10	LK70	*mos2 snc1 npr1*	—
11	LK185	*mos2 snc1 npr1*	—
12	LK98	*mos2 snc1 npr1*	—
13	806	*mos2 snc1 npr1*	—
14	LK24	*mos2 snc1 npr1*	—
15	LK149	*mos2 snc1 npr1*	—
bon1	60B-1	*mos4 snc1*	W100 to Stop
	170	*mos2 snc1 npr1*	G397 to R
	LK40	*mos2 snc1 npr1*	Mutation in intron
cpr1	47-1	*mos4 snc1*	E174 to K
	LK14	*mos2 snc1 npr1*	D264 to N
siz1	68	*mos4 snc1*	R114 to Stop
	LK76	*mos2 snc1 npr1*	W511 to Stop
chs3-3d	17-1	*mos4 snc1*	M1017 to V[10]

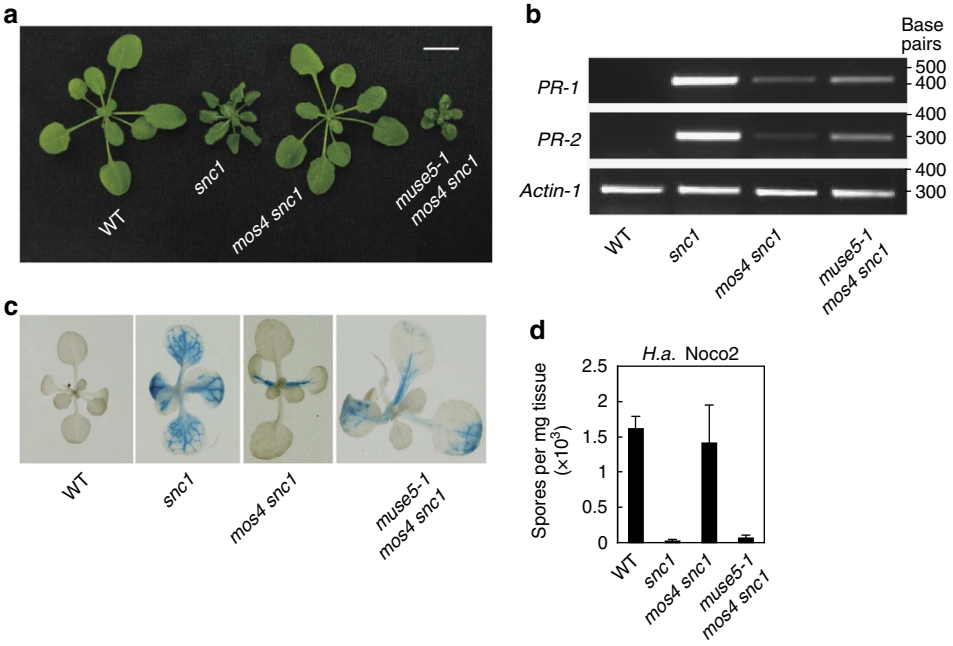

Figure 1 | Characterization of the *muse5-1 mos4 snc1* triple mutant. (**a**) Morphology of 3-week-old soil-grown plants of wild-type (WT), *snc1*, *mos4 snc1* and *muse5-1 mos4 snc1*. Scale bar represents 1cm. (**b**) *PR-1* and *PR-2* expression in WT, *snc1*, *mos4 snc1* and *muse5-1 mos4 snc1* as determined by RT–PCR. Total RNA was extracted from 2-week-old plants grown on 1/2 MS medium and reverse transcribed to cDNA. *PR-1*, *PR-2* and *Actin-1* were amplified by 28 cycles of PCR using equal amounts of total cDNA, and the products were analysed by agarose gel electrophoresis followed by ethidium bromide staining. (**c**) GUS staining of 2-week-old plate-grown seedlings of WT, *snc1*, *mos4 snc1* and *muse5-1 mos4 snc1*. All plants carry the *pPR2::GUS* reporter gene. (**d**) Quantification of *H.a.* Noco2 sporulation on the indicated genotypes. Two-week-old plants were inoculated with *H.a.* Noco2 at a concentration of 10^5 spores per ml of water. The spores were quantified with a hemocytometer 7 days after infection. Bars represent means ± s.d. ($n = 4$ with five plants each). Similar results were obtained in three independent experiments.

in *snc1*. Consistently, the *muse5-1 mos4 snc1* plants showed much stronger *pPR2::GUS* staining than *mos4 snc1* (Fig. 1c). To test whether *muse5-1* alters resistance against a virulent pathogen, *muse5-1 mos4 snc1* seedlings were challenged with the oomycete *H.a.* Noco2. As shown in Fig. 1d, the enhanced resistance response of *snc1* was restored in the triple mutant. Taken together, these results show that *muse5-1* enhances all aspects of *snc1*-mediated autoimmunity in the *mos4 snc1* background.

Positional cloning of *muse5-1*. To identify *muse5-1*, a positional cloning approach was utilized. As *muse5-1 mos4 snc1* is in Columbia (Col) background, the mapping cross was carried out with the original triple mutant and *Landsberg erecta* (*Ler*). The F1 plants were allowed to self-fertilize and 24 F2 plants with similar morphology as *muse5-1 mos4 snc1* were selected as a crude mapping population. The *muse5-1* mutation was mapped to the bottom of chromosome 3 by linkage analysis and was further flanked between markers F24B22 and F2A19 using an additional 72 triple mutant-like F2 plants (Fig. 2a). To create a larger fine mapping population, progeny from several F2 lines heterozygous for the *muse5-1* mutation and homozygous at the *SNC1* locus (*snc1*) and *MOS4* locus (either WT *MOS4* or *mos4*) were used to avoid interference from these two loci. Out of 383 plants from the F3 fine mapping population, 35 recombinants were collected and further analysed using markers between F24B22 and F2A19. The *muse5-1* mutation was eventually mapped between markers F17J16 and T16L24, a distance of 170 kb, which was located on BAC clone F25L23 (Fig. 2a). To find the *muse5-1* mutation, genomic DNA of plants with the *muse5-1 mos4 snc1* genotypes from the mapping population was extracted and sequenced with Illumina whole-genome sequencing. After sequence comparison between the *muse5-1* mutant DNA and the *Arabidopsis* reference genome, only one candidate mutation was found in the mapped region (Supplementary Table S1). Direct Sanger sequencing of the candidate gene using *muse5-1 mos4 snc1* mutant genomic DNA confirmed the G-to-A transition in *At3g59280*, which occurred at an intron–exon splice junction site (Fig. 2b). To test whether this mutation affects the splicing pattern of *At3g59280*, the cDNA of *At3g59280* was amplified by RT–PCR using RNA extracted from both *muse5-1 mos4 snc1* and WT plants. Comparison of the cDNA sequences of *muse5-1* and the WT confirmed an aberrant splicing pattern of *At3g59280* in *muse5-1*, resulting in a G-nucleotide deletion after the start codon (Fig. 2c). As a consequence of the reading frame shift, the MUSE5 protein product is no longer produced.

MUSE5 is a small conserved protein that belongs to the DnaJ chaperon superfamily (Fig. 2d). There is one predicted paralog of *MUSE5* (*At5g61880*, named *MUSE5L*) in *Arabidopsis*. MUSE5 shares 35% amino-acid sequence identity to the *S. cerevisiae* Presequence translocase-associated protein import motor (PAM) subunit PAM16. Alignment of MUSE5, MUSE5L and PAM16 displays the highly conserved PAM16 domain of the proteins (Fig. 2e). Within the PAM16 domain, there is a region of ~85 residues that is denoted as J-like domain (Fig. 2e), which has been shown to be responsible for dimerization with the J domain of PAM18 (refs 11,12).

Confirmation that *MUSE5* is *At3g59280*. Transgenic complementation was carried out to confirm whether the mutation found in *At3g59280* (Fig. 2b) is responsible for enhancing the *snc1* mutant phenotypes. Full-length *At3g59280* genomic DNA

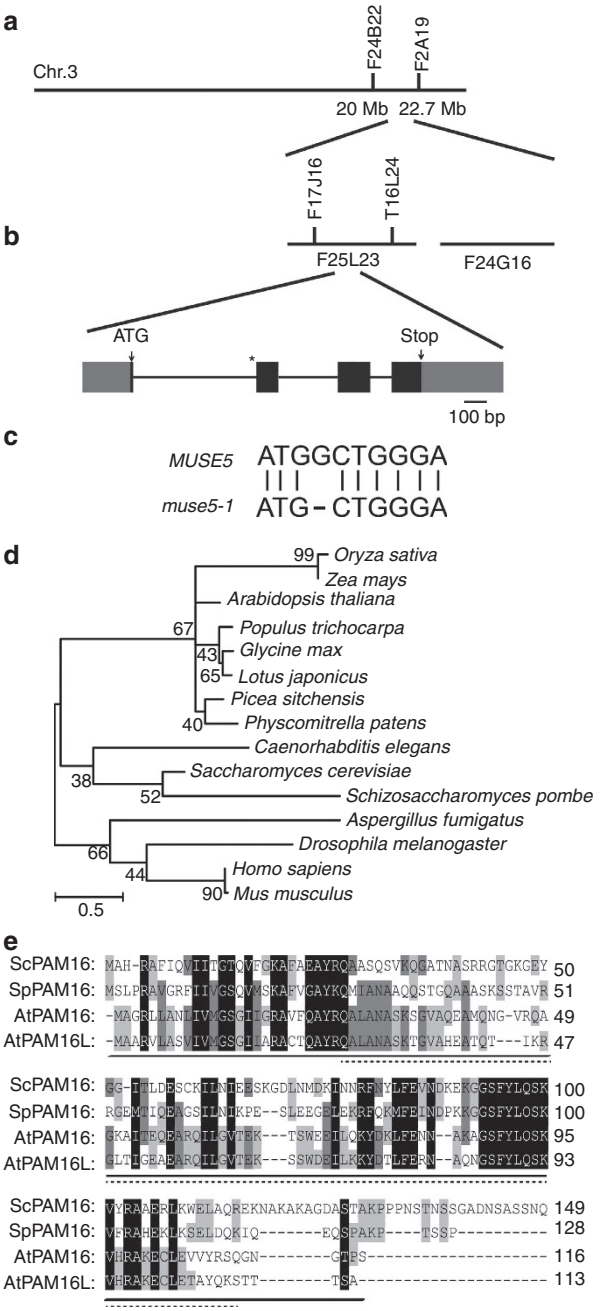

Figure 2 | Positional cloning of *muse5-1*. (**a**) Map position of *muse5-1* on chromosome 3. BAC clones are indicated. (**b**) Gene structure of *MUSE5* (*At3g59280*). Boxes indicate exons and lines indicate introns. Grey regions show the UTRs. The two arrows indicate the start and stop codon, respectively. The asterisk indicates where the G-to-A mutation in *muse5-1* occurred. (**c**) cDNA sequence comparison between *MUSE5* and *muse5-1*. In *muse5-1*, one nucleotide of the third exon was spliced out due to the G-to-A mutation at the intron–exon splice junction that creates a new 3′ splice site, causing a reading frame shift. (**d**) Phylogenetic relationship between PAM16 and its orthologs. The orthologs are represented by the species names. Phylogenetic analysis was carried out using software MEGA v5.05. All amino acid sequences were compiled in FASTA format and used to generate alignment first. Maximum likelihood (ML) tree was implemented assessing with 1,000 bootstrap replications. (**e**) Full-length amino acid sequence alignments of MUSE5, MUSE5L and PAM16 proteins from *S. cerevisiae* (Sc) and *S. pombe* (Sp). The conserved PAM16 domain and degenerate J domain (J-like domain) are underlined by solid and dotted lines, respectively. Black boxes indicate regions in which at least two of three residues are identical and grey boxes indicate conserved residues.

containing 1,067 bp sequence before the start codon was PCR-amplified from WT plants and cloned into a binary vector, which was then transformed into the *muse5-1 mos4 snc1* triple mutant. Six independent transgenic lines all displayed *mos4 snc1*-like morphology. Two representative plants from line #1 and #2 are shown in Fig. 3a. These transgenic plants are slightly smaller than *mos4 snc1* as quantified by whole-plant fresh weight analysis (Fig. 3b). When inoculated with *H.a.* Noco2, these transgenic plants displayed elevated susceptibility as compared with *muse5-1 mos4 snc1* (Fig. 3c). The intermediate phenotypes of these transgenic plants demonstrate that wild-type *At3g59280* can mostly but not fully complement the *muse5-1* defects. This could be due to the missing unknown regulatory elements that were not included in the genomic construct of *At3g59280*.

Previously, *At3g59280* was named *ThaXtomin Resistant 1* (*TXR1*) as mutants of this gene exhibit insensitivity to the cellulose synthesis inhibitor thaxtomin[13]. When we crossed *txr1-1* with *muse5-1 mos4 snc1*, heterozygous F1 plants exhibited *snc1*-like phenotype (Fig. 3d), indicating that *muse5-1* failed to complement *txr1-1*. Taken together, our data suggest that *MUSE5* is *At3g59280*/*TXR1*.

At3g59280/TXR1/MUSE5 is an ortholog of yeast PAM16. TXR1/MUSE5 shares 35% amino-acid sequence identity to the *S. cerevisiae* PAM16 (Fig. 2e), which is a small protein of the inner mitochondrial membrane that is conserved in all fully sequenced eukaryotic genomes. There are two predicted *PAM16* paralogs in *Arabidopsis*, *At3g59280/MUSE5/TXR1* and *At5g61880*. Previously, PAM16, the fifth identified subunit of the PAM, was found to be essential in driving preprotein import into the mitochondrial matrix in *S. cerevisiae*[12]. Thus, a yeast complementation experiment was carried out to determine whether MUSE5 is orthologous to PAM16. The *pam16-1* allele is a temperature-conditional partial loss-of-function yeast strain generated by error-prone PCR, which grows like the wild-type strain at 30 °C but does not grow at 37 °C. At 37 °C, only WT and *pam16-1* cells expressing *TXR1/MUSE5* can grow (Fig. 4a), suggesting that *TXR1/MUSE5* can fully complement the yeast *pam16-1* mutant phenotype. To test whether the yeast PAM16 is also able to complement *muse5*, we cloned yeast *PAM16* and stably expressed it under the control of 35S promoter in *muse5-1 mos4 snc1* triple mutant. As shown in Fig. 4b, the representative transgenic plants revert from *muse5-1 mos4 snc1* to *mos4 snc1*-like morphology. This complementing phenotype indicates that the yeast *PAM16* and *MUSE5* are indeed orthologous. As *TXR1/MUSE5* is an ortholog of yeast *PAM16*, we renamed *At3g59280* as *AtPAM16* and *At5g61880* as *AtPAM16L*. The *muse5-1* allele is renamed *Atpam16-1*, and *txr1-1* is renamed *Atpam16-2*.

AtPAM16 localizes to mitochondrial inner membrane. To identify the subcellular localization of AtPAM16, a construct containing full-length genomic *AtPAM16* DNA, fused with *GFP* at its C terminus and driven by its endogenous promoter containing 1,067 bp sequence before the start codon, was transformed into the *Atpam16-1 mos4 snc1* triple mutant. Similar to expressing *AtPAM16*::*AtPAM16* in the triple background (Fig. 3), expressing *AtPAM16*::*AtPAM16–GFP* in all 12 transgenic lines also mostly complemented the defects of the triple mutant, suggesting that AtPAM16–GFP is functional, although the plants are slightly smaller than *mos4 snc1* (Fig. 5a,b). These transgenic plants displayed similar susceptibility to *H.a.* Noco2 as compared with *mos4 snc1* (Fig. 5c). To investigate the subcellular localization of AtPAM16–GFP *in vivo*, we analysed leaf and root tissues of the transgenic plants by confocal laser scanning microscopy (CLSM). Green fluorescent protein (GFP) fluorescence in both

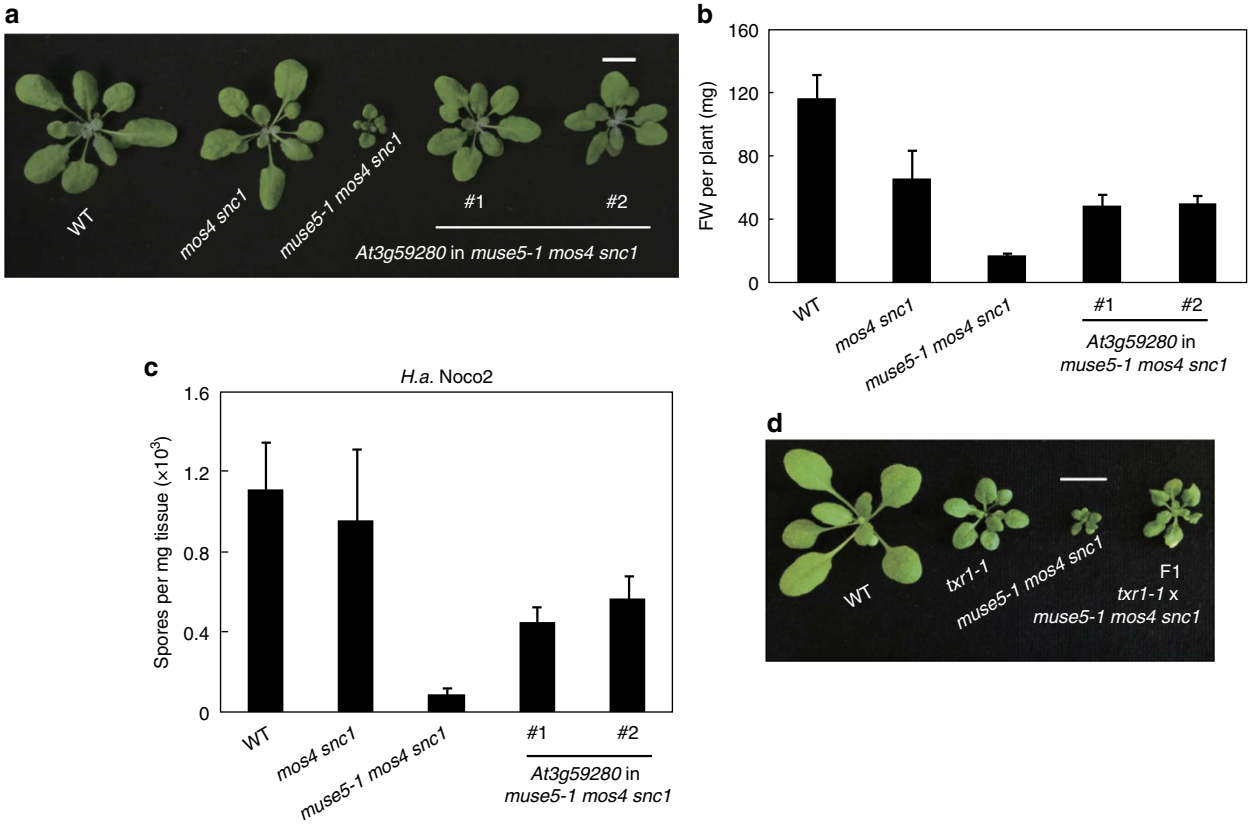

Figure 3 | Confirmation that *MUSE5* is *At3g59280*. (**a**) Plant morphology of WT, *mos4 snc1*, *muse5-1 mos4 snc1* and *muse5-1 mos4 snc1* transformed with a genomic clone of *At3g59280*. Two representative homozygous T3 plants from independent transgenic events are shown. Scale bar is 1 cm. (**b**) Fresh weight (FW) of plants of the indicated genotypes when they are 3-week-old. Bars represent means ± s.d. ($n = 12$). The experiments were repeated three times with similar results. (**c**) Quantification of *H.a.* Noco2 sporulation on the same genotypes as (**a**). Ten-day-old plants were sprayed with *H.a.* Noco2 at a concentration of 10^5 spores per ml of water. The oomycete spores on the surface of leaves were quantified seven days after inoculation. Bars represent means ± s.d. ($n = 4$ with five plants each). Three independent experiments were carried out and similar results were obtained. (**d**) Morphology of plants from the allelism test between *txr1-1* and *muse5-1*. F1 was generated from the cross between *txr1-1* single mutant and *muse5-1 mos4 snc1* triple mutant. Scale bar is 1 cm.

leaf and root cells was observed in punctate structures (Fig. 5d). According to the size and dynamic movement of the AtPAM16–GFP signals within the cells, they are likely to be mitochondria. To confirm mitochondrial localization of AtPAM16, we crossed the transgenic *AtPAM16–GFP* lines with an established mitochondrial marker line stably expressing CFP fused to a mitochondrial targeting sequence (the first 29 amino acids of *S. cerevisiae* cytochrome *c* oxidase IV; mt-ck *CS16262*)[14]. AtPAM16–GFP fluorescence was found to colocalize with mitochondria-targeted CFP (mt-CFP in Fig. 5e) when root cells of F1 plants were examined by CLSM (Fig. 5e). Interestingly, at this higher magnification increased fluorescence was observed at the rim of mitochondria, indicating membrane localization (Fig. 5e).

To test whether AtPAM16–GFP localizes to the inner mitochondrial membrane as does yeast PAM16, we utilized two independent strategies, a biochemical proteinase K digestion assay and a transmission electron microscopy (TEM) immunogold labeling approach using seedlings expressing the native promoter-driven *AtPAM16–GFP*. As shown in Fig. 6a, when isolated intact mitochondria were treated with proteinase K, AtPAM16–GFP was resistant to digestion. However, when the same mitochondria were disrupted by sonication, AtPAM16–GFP could be readily degraded upon proteinase K treatment, as could the mitochondrial inner membrane protein cytochrome *c*. This suggests that AtPAM16–GFP is protected from proteinase K digestion because it is localized inside the mitochondria. In addition, when the same transgenic plants were cryofixed, freeze-substituted and immunolabeled for TEM, quantification of AtPAM16–GPF signal, as detected by a gold-conjugated anti-GFP antibody, revealed significantly more label on mitochondria (mean ± s.e. = 0.00969 ± 0.00064 gold μm^{-2}) as compared with other cellular components (cytoplasm, other organelles, cell wall = 0.00253 ± 0.00016 gold μm^{-2}) in *AtPAM16–GPF* expressing seedlings, or compared with background signal detected in WT samples not expressing the *AtPAM16–GFP* transgene (ANOVA, $P < 0.0001$, $n = 81$ measurements for AtPAM16–GFP, 94 measurements for WT; Fig. 6b,c). This mitochondrial signal was not detected in WT seedlings without the *AtPAM16–GFP* transgene (Fig. 6d) or in *AtPAM16–GFP* seedlings treated without the primary antibody as a control (Fig. 6e).

Taken together, our data suggest that AtPAM16 localizes to the inner membrane of mitochondria like its yeast ortholog PAM16.

Analysis of *Atpam16* single mutants. From the *snc1*-enhancing phenotypes of *Atpam16-1*, we deduced that AtPAM16 probably serves as a negative regulator of *snc1*-mediated immunity. To determine its function in the absence of the *snc1* mutation, we analysed the phenotypes of *Atpam16-1* (*muse5-1*), *Atpam16-2* (*txr1-1*) and *Atpam16l* (*At5g61880*) single mutants. The *Atpam16-1* single mutant was obtained from the F2 generation of

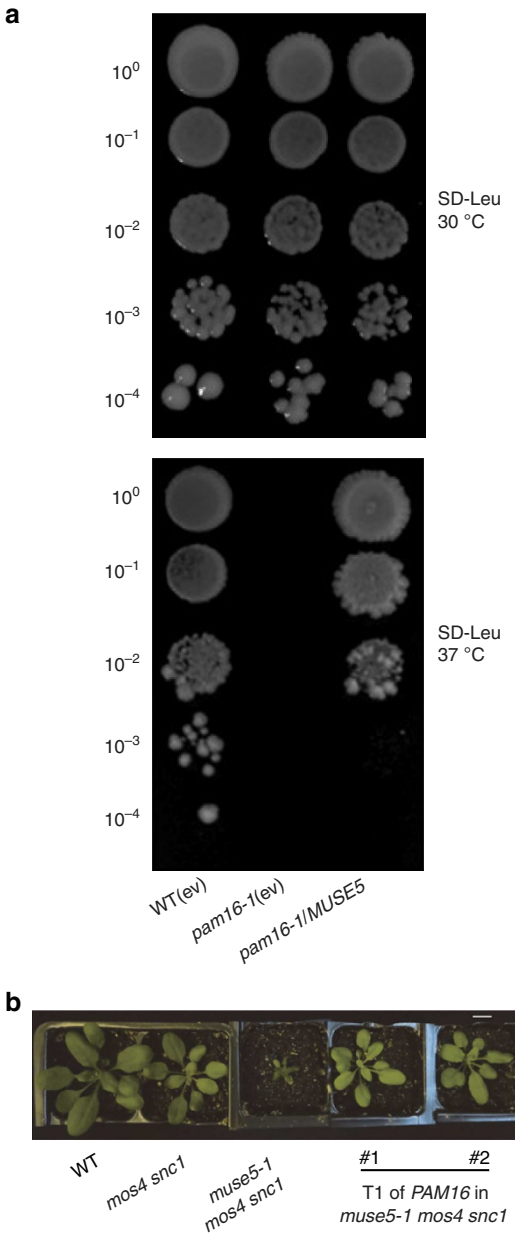

Figure 4 | *AtPAM16* and yeast *PAM16* can complement each other across kingdoms. (**a**) Serial 1/10 dilutions of the following yeast strains containing the same number of cells were plated on SD-Leu medium: left lane, the wild-type (WT) strain expressing empty vector (ev); middle lane, *pam16-1* partial loss-of-function strain expressing empty vector; right lane, *pam16-1* knockout strain expressing *AtPAM16*. Yeast plates were incubated for 3 days at the indicated temperatures before the picture was taken. (**b**) Morphology of WT, *mos4 snc1*, *muse5-1 mos4 snc1* and two representative transgenic T1 plants of *muse5-1 mos4 snc1* transformed with *35S-PAM16*. The plants were 4 weeks old when the picture was taken. Scale bar represents 1 cm.

a cross between *Atpam16-1 mos4 snc1* and WT. We also obtained a T-DNA insertion mutant allele of *AtPAM16L*, which is homologous to *AtPAM16* with 73% similarity (Fig. 2e). This T-DNA mutant (SALK_061634C) contains an insertion in the second exon of *AtPAM16L*, likely leading to truncation of the encoded protein. Compared with WT, *Atpam16-1* and *Atpam16-2* displayed smaller size whereas *Atpam16l* exhibit no obvious morphological defects (Fig. 7a). *Atpam16-2* plants are consistently slightly smaller than *Atpam16-1* plants, suggesting that *Atpam16-2* is a stronger allele than *Atpam16-1*. Single mutant *Atpam16-1*, *Atpam16-2* and *Atpam16l* plants were slightly more resistant to *H.a.* Noco2 compared with WT (Fig. 7b). In addition, when challenged with virulent bacterial pathogen *Pseudomonas syringae* pv. *maculicola* (*P.s.m.*) ES4326, both *Atpam16-1* and *Atpam16-2* exhibit enhanced resistance compared with WT, whereas the susceptibility of *Atpam16l* is similar to WT (Fig. 7c). The relative expression levels of *PR-1* and *PR-2* in these three single mutants were constitutively higher than those in WT (Fig. 7d), with *Atpam16-2* showing the highest expression of these defence marker genes. Taken together, these results indicate that mutations in *AtPAM16* cause enhanced disease resistance.

Mitochondria are sites of ROS production, which is believed to contribute to R protein-mediated immune responses. As AtPAM16 is part of the import motor of mitochondria, we examined ROS levels in the *Atpam16* mutants via luminol-based chemiluminescence assay and DAB staining. As shown in Fig. 7e, upon flg22 PAMP peptide treatment, both alleles of *Atpam16* exhibited higher ROS levels compared with WT and *Atpam16l*, with *Atpam16-2* showing the highest ROS production. A similar trend was observed with DAB staining. Mutant *bir1-1* seedlings were used as positive control, as the mutant accumulates very high levels of hydrogen peroxide, resulting in strong DAB staining[15]. Obvious darker brown staining was observed on *Atpam16-2* seedlings compared with WT (Fig. 7f). The staining is weaker in *Atpam16-1*, consistent with it being a weaker mutant allele of *AtPAM16*. *Atpam16l* displayed much fainter staining that is comparable to that of WT.

We tried to create an *Atpam16-1 Atpam16l* double mutant. Although 200 F2 plants from the cross between *Atpam16-1* and *Atpam16l* were genotyped to screen for the double mutant, no *Atpam16-1 Atpam16l* double mutant could be identified. In the F3 generation obtained from 12 F2 plants heterozygous for *Atpam16-1* and homozygous for *Atpam16l*, we still could not obtain the double mutant, indicating that the double mutant is lethal. As PAM16 is part of the mitochondrial protein import motor, these data suggest that mitochondrial protein import is essential for regular plant development and survival. The lethality of the double mutant also indicates that *AtPAM16* and *AtPAM16L* function redundantly, with *AtPAM16* having a more dominant role in plant immunity as compared with its paralog *AtPAM16L*.

Only *Atpam16-1* and *Atpam16-2* can enhance *snc1*-mediated immunity. To further test the enhancing impact of *AtPAM16* mutations on *snc1*-mediated immune responses, *Atpam16-1 snc1*, *Atpam16-2 snc1* and *Atpam16l snc1* double mutants were generated. Both *Atpam16-1 snc1* and *Atpam16-2 snc1* exhibited *snc1*-enhancing stunted growth compared with *snc1*, whereas *Atpam16l snc1* is indistinguishable from *snc1* (Fig. 8a). All three double mutants were more resistant to the oomycete pathogen *H.a.* Noco2 compared with WT (Fig. 8b). Thus, *snc1*-mediated immune response can only be enhanced by *Atpam16-1* and *Atpam16-2*, but not by *Atpam16l*.

Discussion

During the past two decades, many genetic screens have been targeting towards finding negative regulators of plant immunity. For example, early screens aiming at the isolation of mutants showing accelerated cell death (ACD) and lesions simulating disease (LSD) resistance identified components that are responsible for cell death or HR suppression[16,17]. Additional mutations in negative regulators were identified from defence marker-assisted screens such as the constitutive expression of *PR* genes (CPR) screen using *pPR2-GUS* and the constitutive immunity

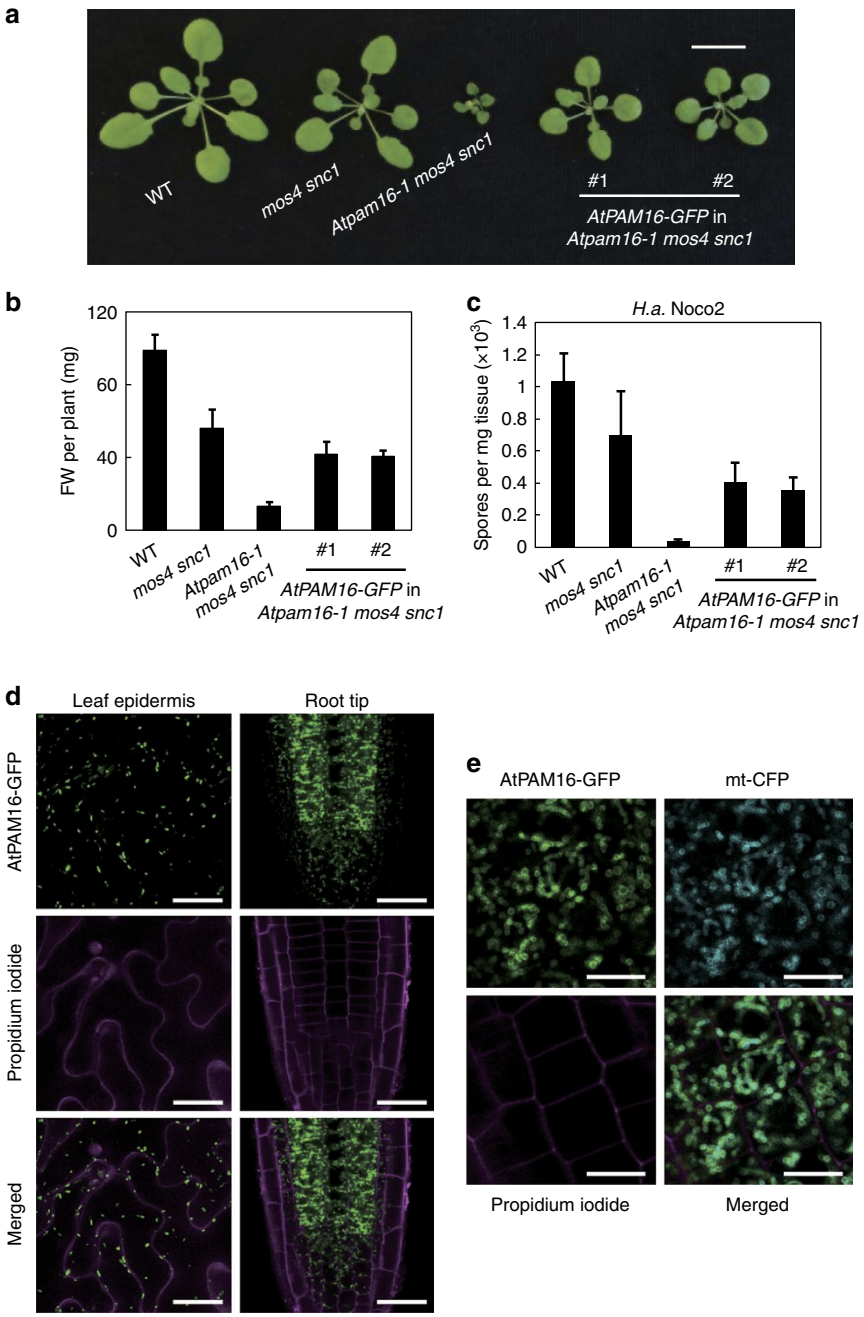

Figure 5 | AtPAM16-GFP localizes to the mitochondrial membrane. (**a**) Morphology of WT, *mos4 snc1*, *Atpam16-1 mos4 snc1* and *Atpam16-1 mos4 snc1* transformed with *AtPAM16-GFP*. Two representative homozygous T3 plants from independent transgenic lines are shown. Scale bar is 1 cm. (**b**) Fresh weight (FW) of 3-week-old plants of the indicated genotypes. Bars represent means ± s.d. ($n = 12$). The experiments were repeated three times with similar results. (**c**) Quantification of *H.a.* Noco2 sporulation on the same genotypes as Fig. 5a. Ten-day-old seedlings were inoculated with a conidiospore suspension of 10^5 spores per ml of water. Spores were counted 1 week after inoculation. Bars represent means ± s.d. ($n = 4$ with 5 plants each). Three independent experiments were carried out with similar results. (**d**) Confocal images of AtPAM16-GFP fluorescence in leaf pavement and root cells of soil-grown *Atpam16-1 mos4 snc1* transgenic plants expressing *AtPAM16-GFP* under control of the native *AtPAM16* promoter. Cell walls were stained with propidium iodide to visualize the outlines of cells. Scale bars are 20 μm. (**e**) AtPAM16-GFP colocalizes with CFP fused to a mitochondrial targeting sequence. Confocal fluorescence microscopy images of root cells of soil-grown F_1 plants grown from a cross between a transgenic plant expressing *AtPAM16-GFP* under its native promoter in the *Atpam16-1 mos4 snc1* background and a transgenic marker line expressing CFP fused to a 29-amino acid mitochondrial (mt) targeting sequence of *S. cerevisiae* cytochrome *c* oxidase IV[14]. Cell walls were stained with propidium iodide to visualize the outlines of cells. Scale bars are 10 μm. At this higher magnification, the image is a bit blurry due to fast movements of the mitochondria.

(CIM) screen based on the *pPR1*-luciferase reporter activity[18,19]. Suppressor screens with different *npr1* mutant alleles were independently carried out in suppressor of *npr1*, inducible (SNI), suppressor of *npr1*, constitutive (SNC) and suppressor of SA insensitivity (SSI) screens, which identified a number of negative regulators dependent or independent of NPR1 (refs 4,20–22). Although these screens have been exhaustive in generating mutants that exhibit extreme constitutive immune

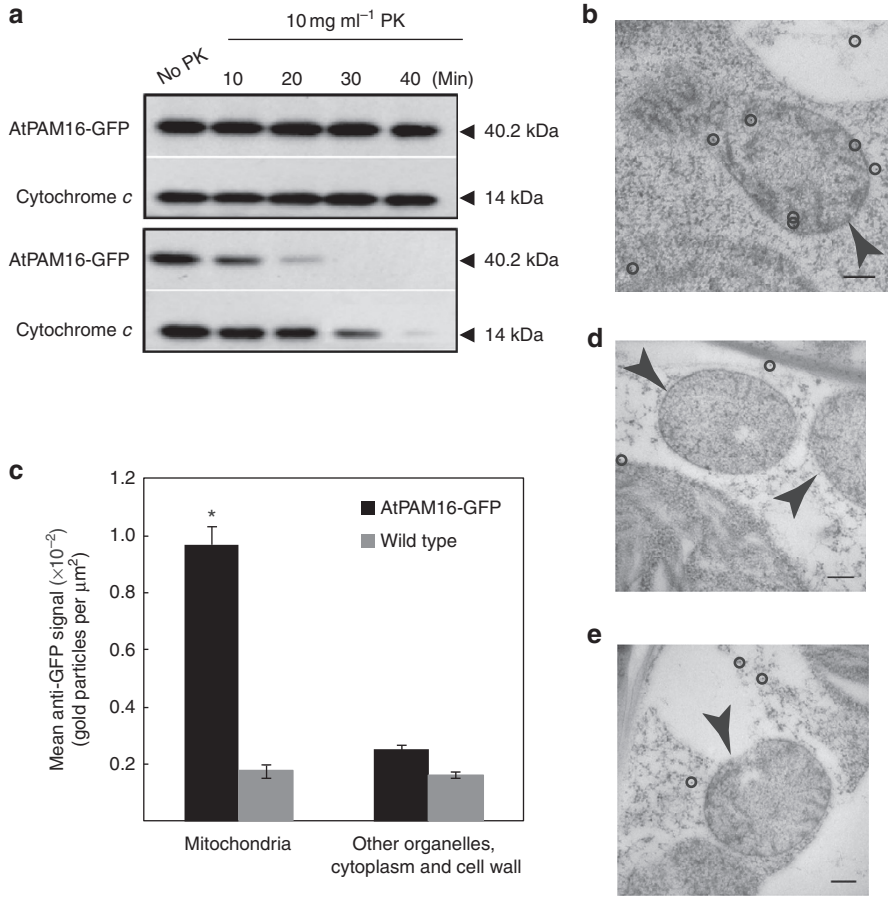

Figure 6 | AtPAM16-GFP localizes to mitochondria inner membrane. (**a**) Immunodetection of AtPAM16-GFP from isolated mitochondria treated with proteinase K. Intact mitochondria (top panel) or sonication-ruptured mitochondria (lower panel) were treated with 10 mg ml^{-1} proteinase K (PK). Cytochrome *c*, a known mitochondria inner membrane protein, was used as positive control. (**b**) Immuno-TEM using a gold-conjugated anti-GFP antibody to detect AtPAM16-GFP. Arrowhead points to mitochondrion, circles highlight gold particles, scale bar represents 200 nm. (**c**) Quantification of mitochondrial signal relative to background signal in cytoplasm, other organelles and the cell wall revealed significantly more gold per μm^2 in mitochondria (ANOVA, $P<0.0001$, $n=81$ AtPAM16-GFP, $n=94$ wild type). * indicates a statistically significant difference, error bars represent s.e. (**d**) Col-0 seedlings without the AtPAM16-GFP transgene treated with anti-GFP. Arrowheads point to mitochondria, circles highlight gold particles, and scale bar represents 200 nm. (**e**) The AtPAM16-GFP inner mitochondrial membrane signal was not detected in AtPAM16-GFP seedlings treated without a primary antibody. Arrowhead points to mitochondrion, circles highlight gold particles and scale bar represents 200 nm.

responses, such as lesion mimic or extremely dwarfed plants, negative regulators that do not exhibit severe morphological defects when mutated have not been targeted using a genetic approach. This is partly due to technical difficulties in identifying the mutation with traditional map-based cloning approaches.

Here, we describe our mutant, *snc1*-enhancing (MUSE) genetic screen, intending to identify negative regulators that do not necessarily show dramatic autoimmunity defects when mutated. This screen is a modified version of a *snc1* enhancer screen in which we are particularly interested in mutants that show minor phenotypes by themselves, but are able to drastically enhance *snc1*-mediated autoimmunity. These mutants may reveal a large number of missing negative regulators in plant immune regulatory pathways. The usage of the unique *snc1* mutant not only provides us with a sensitized background to reveal mild enhanced-resistance phenotypes of the *muse* mutants, it also enables convenient phenotyping during further genetic mapping. In order to avoid possible lethality of the *snc1 muse* double mutants due to enhanced autoimmunity, we utilized plants with *mos2* or *mos4* in the *snc1* background that grow to wild-type size and morphology despite the *snc1* mutation[7,9].

As a proof of concept, we identified several mutant alleles of three well-known negative regulators of plant immunity, *BON1*, *CPR1* and *SIZ1* (Table 1). We also identified a rare gain-of-function *chs3-3d* allele[10] and several intragenic second-site gain-of-function alleles of *snc1*, which will be reported elsewhere. Both *BON1* and *CPR1* are genetically dependent on *SNC1*[23–25]. BON1 regulates *SNC1* transcription through unknown mechanisms, whereas SCF^{CPR1} directly targets SNC1 and other NB-LRR proteins for degradation[24,25]. The SUMO E3 ligase SIZ1 is involved in the regulation of many biological processes, one of which is the negative regulation of defence hormone salicylic acid (SA) accumulation[26,27]. However, the exact role of SIZ1 in the regulation of SA signalling is unclear.

Aside from these known negative regulators of plant immunity, most of the *muse* mutants we identified so far seem to carry mutations in novel genes as they do not map to known negative regulators of plant disease resistance. Future cloning and detailed biochemical studies of these *MUSE* genes and their encoded proteins, one of which (MUSE5/AtPAM16) is described here, will enable us to better understand negative regulatory mechanisms that help fine-tune plant immunity.

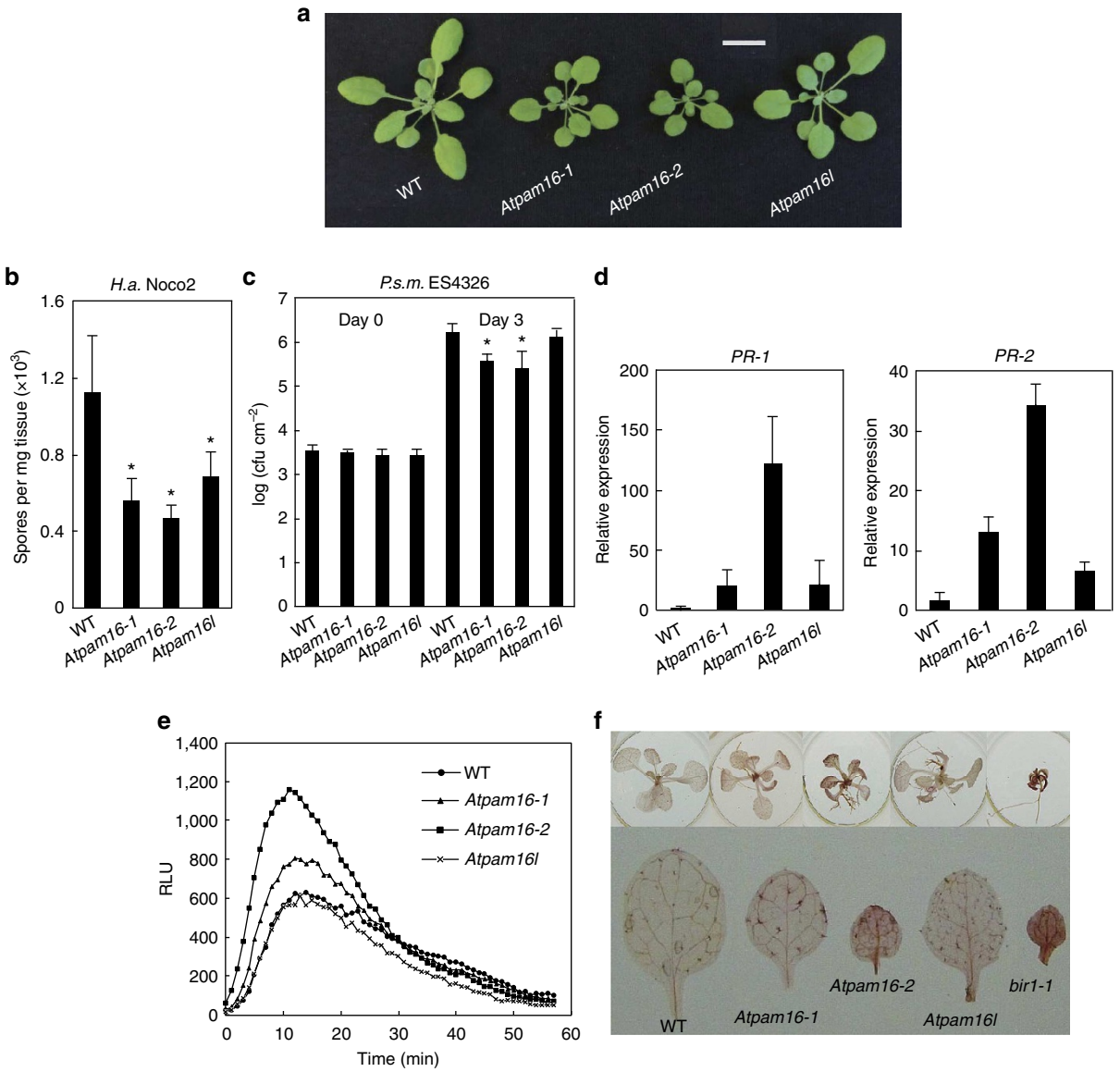

Figure 7 | Single mutant analysis of *Atpam16* and *Atpam16l*. (**a**) Morphology of WT, *Atpam16-1*, *Atpam16-2* and *Atpam16l* single mutants. The picture was taken from soil-grown plants when they were 3 weeks old. Scale bar represents 1 cm. (**b**) Quantification of *H.a.* Noco2 sporulation in WT, *Atpam16-1*, *Atpam16-2* and *Atpam16l* seedlings. Two-week-old plants were inoculated with *H.a.* Noco2 at a concentration of 10^5 spores per ml of water. The oomycete spores on the surface of leaves were counted 7 days after inoculation. Bars represent means ± s.d. ($n = 4$ with 5 plants each). The experiment was repeated three times and similar results were observed. Asterisks indicate significant differences of *Atpam16-1*, *Atpam16-2* and *Atpam16l* compared with WT based on Student's *t* test, $P < 0.05$ (*). (**c**) Bacterial growth of *P.s.m.* ES4326 in WT, *Atpam16-1*, *Atpam16-2* and *Atpam16l*. Leaves of 4-week-old plants were infiltrated with a bacterial suspension at $OD_{600} = 0.0005$. Leaf discs within the infected area were taken at day 0 and day 3 to quantify colony-forming units (CFU). Bars represent means ± s.d. ($n = 5$). Asterisks indicate significant differences of *Atpam16-1*, *Atpam16-2* and *Atpam16l* compared with WT based on Student's *t* test, $P < 0.05$ (*). (**d**) Relative expression of *PR-1* and *PR-2* in WT, *Atpam16-1*, *Atpam16-2* and *Atpam16l* as determined by real-time RT-PCR. Total RNA was extracted from 4-week-old plants grown on soil and reverse transcribed to cDNA. Both *PR-1* and *PR-2* expression levels were normalized by *Actin-1*. Bars represent means ± s.d. ($n = 3$). The experiment was repeated three times with similar results. (**e**) Oxidative burst in response to flg22 in WT, *Atpam16-1*, *Atpam16-2* and *Atpam16l*. Under 12 h light/12 h dark cycle growth condition, leaf slices of 4-week-old plants were treated with 1 μM flg22 as elicitor. Oxidative burst was indirectly measured as relative light units (RLU) using a luminol-based chemiluminescence assay[38]. Three independent experiments ($n = 10$) were performed with similar results. (**f**) DAB staining of 2-week-old 1/2 MS plate-grown plants of WT, *Atpam16-1*, *Atpam16-2* and *Atpam16l*. The whole plants and representative leaves are shown. Mutant *bir1-1* was used as positive control.

Much of the mitochondrial protein import mechanism has been uncovered from studies using yeast. In eukaryotes, >98% of mitochondrial proteins are nuclear-encoded and ~10–15% of nuclear genes encode mitochondrial proteins that need to be either incorporated into the organelle membrane or imported into the matrix. Proteins targeted to the mitochondrial matrix need to be transported by two distinct transport machineries. The TOM complex transfers proteins across the mitochondrial outer membrane, whereas the TIM23 complex transports the protein through the inner membrane[28,29]. PAM16 is part of the import motor of the TIM23 complex that facilitates the import of preproteins together with the mtHSP70 proteins and the co-chaperones Mge1, Tim44 and Pam18. It forms a stable heterodimer with PAM18 and resides on the matrix-side of the

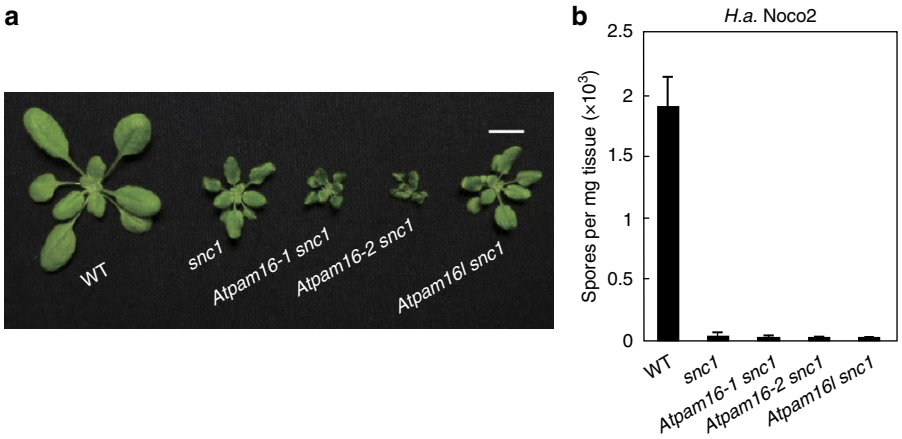

Figure 8 | Analysis of *Atpam16 snc1* double mutants. (**a**) Plant morphology of WT, *snc1*, *Atpam16-1 snc1*, *Atpam16-2 snc1* and *Atpam16l snc1*. The picture was taken of soil-grown plants when they were 3 weeks old. Scale bar is 1 cm. (**b**) Quantification of *H.a.* Noco2 sporulation in WT, *snc1*, *Atpam16-1 snc1*, *Atpam16-2 snc1* and *Atpam16l snc1* seedlings. Two-week-old seedlings were sprayed with *H.a.* Noco2 at a concentration of 10^5 spores per ml of water. The spores were quantified 1 week after infection. Bars represent means ± s.d. ($n = 4$ with five plants each). Similar results were observed in three independent experiments.

mitochondrial inner membrane[30]. In yeast *pam16* mutants, preprotein import into the matrix is defective[12]. The analogous and vital preprotein import function of PAM16 in *Arabidopsis* is supported by our data that *Atpam16 Atpam16l* double mutant plants are lethal. The conservation of the mitochondrial protein import machinery is also reflected by the fact that most of the TOM and TIM23 complex member-encoding genes can be found in *Arabidopsis* and other higher eukaryotes.

Using a combination of traditional mapping and next-generation sequencing, we identified *MUSE5* as *AtPAM16*. Several lines of evidence indicate that AtPAM16 is an ortholog of the yeast mitochondrial inner membrane protein import motor PAM16. First, *AtPAM16* is able to fully complement a yeast temperature-conditional *pam16* allele (Fig. 4a), while the yeast *PAM16* is able to complement *Atpam16* defects (Fig. 4b). These complementation data indicate that PAM16 is functionally highly conserved among eukaryotes, agreeing with the sequence analysis of *PAM16*-encoding genes in different organisms (Fig. 2d). Additionally, in *Arabidopsis*, expression of the *AtPAM16–GFP* fusion gene construct complements the *Atpam16* defects, suggesting that the fusion protein localizes to the proper subcellular compartment. Indeed, confocal fluorescence microscopy confirmed that AtPAM16–GFP localizes to mitochondrial rims (Fig. 5d,e), supporting its predicted function as part of the mitochondrial inner membrane protein import motor. In addition, our cryo-TEM and proteinase K digestion assay suggest that AtPAM16 indeed localizes to the inner membrane of mitochondria (Fig. 6a–c).

Previously, an *Atpam16-2* mutant allele (named *txr1-1*) was identified from a forward genetic screen searching for thaxtomin A-resistant mutants[13]. Thaxtomin A is a phytotoxin from *Streptomyces* species, in particular *Streptomyces scabies*, the causal agent of potato scab. Application of thaxtomin A at a concentration as low as 50 nM causes *Arabidopsis* seedlings to exhibit severe growth retardation as a consequence of cellulose synthesis inhibition[13]. The strong effect of thaxtomin A on cellulose synthesis is intriguing[13,31]. One interesting observation Bischoff *et al.*[31] made is that application of thaxtomin enhances *PR* gene expression (Fig. 2 in the study of Bischoff *et al.*[31]), which is in agreement with the heightened *PR* gene expression of *Atpam16* mutants (Fig. 7d). As our analysis revealed that TXR1 is actually AtPAM16, an alternative model of thaxtomin A's mode of action is proposed. It is possible that the cellulose synthesis defects are downstream of its primary toxicity on mitochondria. Thaxtomin A may be targeting a mitochondrial matrix protein that relies on AtPAM16 for import or it could be directly targeting AtPAM16 itself. Such targeting may serve as a virulence strategy to release a death signal from mitochondria and assists the killing of host cells so that the pathogen can consume the plant's photosynthates. The thaxtomin-resistant phenotype of *Atpam16* mutant plants is in agreement with this hypothesis. In *Atpam16* mutant plants, this thaxtomin target may no longer be effectively imported into the matrix, thus exhibiting a thaxtomin-resistant phenotype. Future analysis on the effect of the phytotoxin on mitochondria will reveal more accurate relationships between the two.

How does AtPAM16 as part of the mitochondrial inner membrane import motor regulate plant immunity? Mitochondria have long been connected with the HR, a programmed cell death event that is associated with R protein-mediated immunity. It has been shown that mitochondria release the death signal cytochrome *c* to the cytosol, leading to the initiation of cell death and subsequent release of molecules such as ROS that drive the destruction of the cell[32]. Multiple sources and types of ROS are involved in HR development, and it is generally believed that these are directed against pathogens[33]. Mitochondria are among the multiple organelles that contribute to ROS production. Mutants defective in mitochondrial ROS (mROS) generation exhibit enhanced disease susceptibility to specific fungal and bacterial pathogens[34]. All these studies point to a positive regulatory role of mitochondria during immune responses through ROS generation.

Intriguingly, our mutant analysis of *Atpam16* alleles suggests that the positive role of mitochondria in ROS production is negatively regulated. Mutations in *Atpam16-1* and *Atpam16-2* enhance *snc1*-mediated autoimmunity (Figs 1 and 8). Single mutants *Atpam16-1*, *Atpam16-2* and *Atpam16l* display an enhanced disease resistant phenotype and higher level of *PR-1* and *PR-2* expression (Fig. 7b–d). *Atpam16* single mutants also exhibit elevated ROS level (Fig. 7e,f). These observations suggest that AtPAM16 functions in negative regulation of plant immunity through repressing mROS production. As AtPAM16 is part of the mitochondrial protein import motor, this regulatory role is probably not direct. We propose that AtPAM16 is involved in the import of a nuclear-encoded negative regulator of plant immunity into the mitochondrial matrix, along with other protein targets.

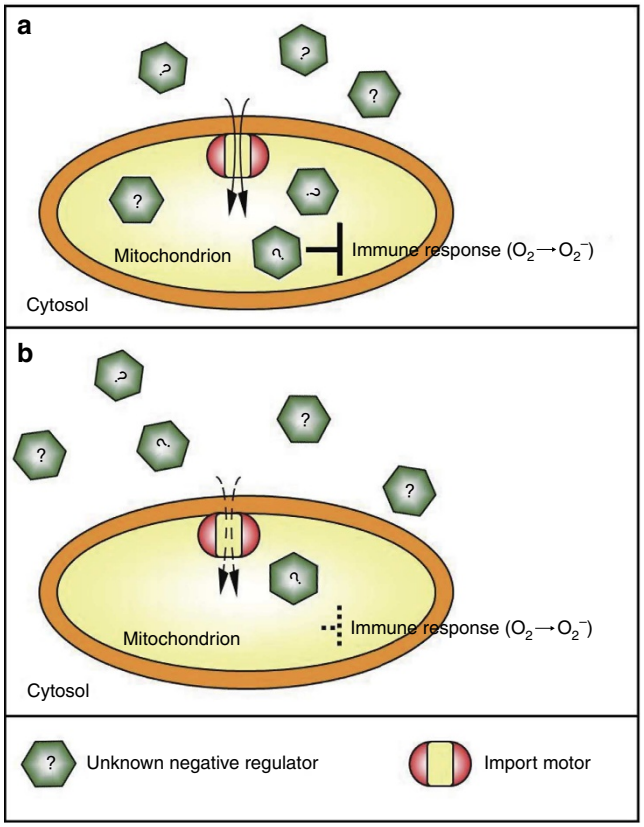

Figure 9 | Model of AtPAM16 as a subunit of mitochondria inner membrane import motor for negative regulation of plant immunity. (**a**) AtPAM16 normally facilitates import of an unknown negative regulator (?) into mitochondria during an immune response. This inhibition helps to prevent autoimmunity due to uncontrolled immune response, such as over-production of ROS. (**b**) With a mutation in AtPAM16, this negative regulator cannot be fully imported into mitochondria, thus leading to autoimmunity and ROS accumulation due to insufficient repression. Partial import of this negative regulator can still be achieved through AtPAM16L.

This negative regulator is responsible for repressing processes such as excessive mROS production, which may lead to autoimmunity or unwanted cell death that would be detrimental to the plant (Fig. 9a). Mutations in *AtPAM16* may therefore attenuate the import of this negative regulator, leading to enhanced immunity (Figs 7 and 9b).

In summary, the plant mitochondria inner membrane import motor AtPAM16 was identified as an important contributor to R protein-mediated immunity, as well as an essential protein in plant survival. This work highlights the significance of negative regulation of mitochondrial activity in plant immunity. Future identification of the AtPAM16 targets will reveal further mechanistic details of how this negative regulation is achieved.

Methods

Plant growth conditions and mutant screens. All plants were grown in climate-controlled chambers under long day conditions (16 h light/8 h dark cycle) at 22 °C. Approximately 10,000 *mos4 snc1* mutant seeds were treated with 20 mM ethyl methanesulfonate (EMS) for 18 h. Roughly 50,000 M2 plants representing ~2,500 M1 families were grown on soil and screened for *snc1*-like morphology. Seeds of putative mutants were plated on 1/2 MS medium and tested for constitutive *pPR2-GUS* reporter gene expression by GUS staining. Mutants with constitutive GUS staining were further analysed by *H.a.* Noco2 infection.

Gene expression analysis. About 0.07 g tissue was collected from 2-week-old seedlings grown on 1/2 MS medium and RNA was extracted using the Totally RNA kit (Ambion,). Superscript II reverse transcriptase (Invitrogen) was used to reverse transcribe 0.4 µg total RNA to generate cDNA. cDNA samples were initially normalized with *ACTIN* by real-time PCR using the QuantiFAST SYBR Green PCR kit. The cDNA was subsequently amplified by PCR using 94 °C for 2 min and cycles of 94 °C for 20 s, 58 °C for 30 s and 68 °C for 1 min. The sequences of primers used are: *PR-1*F, 5′-GTAGGTGCTCTTGTTCTTCCC-3′ and *PR-1*R, 5′-CACATAATTCCCACGAGGATC-3′; *PR-2*F, 5′-GCTTCCTTCTTCAACCA CACAGC-3′ and *PR-2*R 5′-CGTTGATGTACCGGAATCTGAC-3′; *Actin-1*-F, 5′-CGATGAAGCTCAATCCAAACGA-3′ and *Actin-1*-R, 5′-CAGAGTCGAGCA CAATACCG-3′.

Pathogen infections. Infection of *H.a.* Noco2 was performed on 2-week-old soil-grown seedlings sprayed with a concentration of 10^5 spores per ml of water. The inoculated seedlings were subsequently kept in a growth chamber with high humidity (~80%) at 18 °C under 12 h light/12 h dark cycle for 7 days before the growth of *H.a.* Noco2 was quantified by counting spores. For infections with *P.s.m.* ES4326, 5-week-old soil-grown plants were infiltrated with bacterial suspension ($OD_{600} = 0.0005$) in 10 mM $MgCl_2$. Leaf punches were taken at day 0 and day 3. Colony-forming units were determined after serial dilution and bacterial incubation at 28 °C on LB plates[5].

Positional cloning and Illumina whole-genome sequencing. Triple mutant *muse5-1 mos4 snc1* plants were crossed with WT *L. erecta*. Crude mapping was performed on F2 plants homozygous for *muse5-1* and fine mapping was performed on F3 plants derived from F2 plants heterozygous for *muse5-1* and homozygous for *mos4* and *snc1*. Both the phenotype and genotype of the recombinants were confirmed in the next generation. The markers used to map *muse5-1* were designed according to the insertion and deletion polymorphisms between the genomic sequences of Col and Ler ecotypes, provided by Monsanto on TAIR (http://www.arabidopsis.org).

Once the *muse5* mutation was narrowed down to a small region of ~1 Mb, the genomic DNA of seedlings of the *muse5-1 mos4 snc1* genotype from the mapping population were sequenced with Illumina whole-genome sequencing following the NEB Instruction Manual of 'NEB Next DNA Library Prep Master Mix Set for Illumina'. Briefly, the purified genomic DNA was sonicated into fragments of ~300 bp. which were set to end-repair, dA-tailing and adaptor ligation. After removal of unligated adaptors, the ligated DNA was enriched by PCR to create a genomic DNA library. Then, the genomic DNA library was sequenced using an Illumina Genome Analyzer. After comparison with WT genomic sequence, the mutations within the flanking area were selected for further analysis. The sequences of primers for PCR are: P1, 5′-AATGATACGGCGACCACCGAGATCTACACT CTTTCCCTACACGA-3′; P2, 5′-CAAGCAGAAGACGGCATACGAGCTCTTCC GATCT-3′.

Transgenic complementation. A transgenic complementation experiment was conducted to confirm that the mutation identified in *At3g59280/TXR1* is *muse5-1*. Full-length *At3g59280/TXR1/AtPAM16* genomic DNA including 1,067 bp of native promoter sequence was amplified by PCR, cloned into the pCAMBIA1305 vector and transformed into *muse5-1 mos4 snc1* plants by the floral dipping method[35]. Transgenic plants from the T2 generation were selected on 1/2 MS plates containing 50 mg ml^{-1} of hygromycin to identify homozygous lines. The construct used for TXR1/MUSE5/AtPAM16–GFP analysis was created in the same way but with a vector containing a GFP tag. Seeds of *txr1-1* were generously provided by Dr Wolf-Rüdiger Scheible. For allelism test between *txr1-1* and *muse5-1*, *txr1-1* was crossed with *muse5-1 mos4 snc1* to generate F1. Morphologic phenotypes of F1 plants were examined.

Confocal microscopy. Confocal images of *AtPAM16–GFP* and *mt-CFP* transgenic seedlings were obtained with a Leica SP5 confocal microscope (Leica GmbH, Wetzlar, Germany) at 488 nm excitation for GFP (500–540 nm emission, HyD3 detector), at 548 nm excitation for CFP (465–485 nm emission) and at 561 nm excitation for the detection of propidium iodide (600–640 nm emission), which was used at a concentration of 0.05% in H_2O for staining cell walls.

Yeast plasmids. Wild-type *TXR1/MUSE5* cDNA was PCR-cloned into yeast expression vector p425-GPD, using *Bam*HI and *Sal*I restriction sites for inserting *AtPAM16* behind the GPD promoter. The previously created *pam16-1* mutant was kindly provided by Dr Peter Rehling[12].

Mitochondria isolation and proteinase K digestion assay. Mitochondria from *AtPAM16–GFP* transgenic plants were isolated according to a previously established procedure (http://www.edvotek.com/Plants). Briefly, 2-week-old plate-grown seedlings (5 g) were harvested and ground to a fine powder in liquid nitrogen and mixed with 10 ml cold lysis buffer (20 mM Tris-HCl, pH 7.4, 25% glycerol, 20 mM KCl, 2 mM EDTA, 2.5 mM $MgCl_2$, 250 mM sucrose and 1 mM PMSF). The homogenate was filtered through a 95-µm and 40-µm nylon mesh sequentially. The flow-through was spun at 4 °C, 700 g for 10 min to pellet the

nuclei and cell debris. The supernatant was transferred and centrifuged at 10,000 *g* for 10 min at 4 °C. The pellet at the bottom is enriched with intact mitochondria. The pellet was further washed using suc washing buffer (0.3 M sucrose, 10 mM Tris, 0.2% BSA) and centrifuged at 10,000 *g* for 10 min at 4 °C to obtain relatively pure mitochondria. The isolated mitochondria were resuspended in 100 µl of 0.4 M Suc, 50 mM Tris, 3 mM EDTA, 0.1% (*w*/*v*) BSA, pH 7.5. The mitochondria suspension was further subjected to 10 mg ml^{-1} proteinase K digestion. Samples were incubated on ice for 10, 20, 30 and 40 min individually before adding 35 µl 4 × Laemmli loading buffer and heated at 95 °C for 5 min. Sonication-disrupted mitochondria solution was used as control for proteinase K digestion. The full western blots are shown in Supplementary Fig. S1.

Cryofixation immune-gold labelling for TEM. *AtPAM16–GFP* transgenic plants were used in cryo-TEM for subcellular localization. Seven-day-old seedlings were high-pressure-frozen in 1-hexadecene in B-type sample holders (Ted Pella) using a Leica HPM-100. Samples were freeze-substituted in 0.1% uranyl acetate, 0.25% glutaraldehyde and 8% dimethoxypropane in acetone for 5 days, then brought to room temperature and infiltrated with LR white resin (London Resin Company) over 4 days. Immunolabeling was performed according to McFarlane *et al.*[36], using 1/100 anti-GFP (Invitrogen A6455) and 1/100 goat-anti-rabbit conjugated to 10 nm gold (Ted Pella). Samples were viewed using a Hitachi 7600 TEM at 80 kV accelerating voltage with an AMT Advantage CCD camera (Hamamatsu ORCA). AtPAM16–GFP signal was quantified relative to background by counting the number of gold particles per µm^2 of mitochondria relative to the gold per µm^2 of other cellular contents (cytoplasm, other organelles and cell wall) using ImageJ. Mean gold per µm^2 was compared between mitochondria and the rest of the cell in AtPAM16–GFP and WT without the transgene using ANOVA ($n = 81$) measurements from eight independent seedlings from two independent transgenic AtPAM16–GFP lines, and 94 measurements from WT.

Creating mutants. To identify the *Atpam16-1* single mutant, *Atpam16-1 mos4 snc1* was crossed with WT containing *pPR2-GUS*. F2 plants were genotyped for the *Atpam16-1*, *mos4* and *snc1* loci by genotype-specific PCR. Lines homozygous for *Atpam16-1* without *mos4* and *snc1* mutations were regarded as *Atpam16-1* single mutants. Lines homozygous for *Atpam16-1* and *snc1* with no *mos4* mutation were kept as *Atpam16-1 snc1* double mutants.

T-DNA insertion mutant *Atpam16l* was obtained from the Arabidopsis Biological Resource Centre (ABRC). Plants homozygous for the T-DNA insertions were identified by PCR. To create the *Atpam16-1 Atpam16l* double mutant, *Atpam16-1* single mutant was crossed with *Atpam16l*. In the F2 generation, ~200 plants were genotyped by PCR.

The *Atpam16-2 snc1* and *Atpam16l snc1* double mutants were obtained by crossing *Atpam16-2* or *Atpam16l* to *snc1* and the double mutants were identified in F2 by genotyping.

DAB staining. DAB staining was performed on 2-week-old seedlings grown on 1/2 MS medium, following a previously described procedure.[37] Briefly, the seedlings were soaked with 2 ml DAB solutions (1 mg ml^{-1} DAB, 0.05% *v*/*v* Tween 20 and 10 mM sodium phosphate buffer (pH 7.0)) in a 24-well tissue culture plate and vacuumed for 2 minutes before incubating on an orbital shaker. After 1-hour incubation, the staining solution was removed and the samples were destained with 95% ethanol and examined by microscopy for brown deposition.

Oxidative burst detection. ROS production from leaves was measured with a previously reported luminol-based assay[38]. In brief, plants were grown in climate-controlled chambers under 12 h light/12 h dark cycles at 22 °C. Leaves of 4-week-old soil-grown plants were sliced into ~1 mm segments and floated in wells overnight on H_2O under light. H_2O was replaced with reagent containing luminol, peroxidase and flg22. ROS released by leaf tissue was detected by luminescence of luminol.

References

1. Dangl, J. L. & Jones, J. D. Plant pathogens and integrated defence responses to infection. *Nature* **411,** 826–883 (2001).
2. Chisholm, S. T., Coaker, G., Day, B. & Staskawicz, B. J. Host-microbe interactions: shaping the evolution of the plant immune response. *Cell* **124,** 803–814 (2006).
3. Maekawa, T., Kufer, T. A. & Schulze-Lefert, P. NLR functions in plant and animal immune systems: so far and yet so close. *Nat. Immunol.* **12,** 817–826 (2011).
4. Li, X., Clarke, J. D., Zhang, Y. & Dong, X. Activation of an EDS1-mediated R-gene pathway in the snc1 mutant leads to constitutive, NPR1-independent pathogen resistance. *Mol. Plant Microbe Interact.* **14,** 1131–1139 (2001).
5. Zhang, Y., Goritschnig, S., Dong, X. & Li, X. A gain-of-function mutation in a plant disease resistance gene leads to constitutive activation of downstream signal transduction pathways in suppressor of npr1-1, constitutive 1. *Plant Cell* **15,** 2636–2646 (2003).
6. Johnson, K. C., Dong, O. X., Huang, Y. & Li, X. A Rolling Stone Gathers No Moss, but Resistant Plants Must Gather Their MOSes. *Cold Spring Harb. Symp. Quant. Biol.* **77,** 259–268 (2012).
7. Palma, K. *et al.* Regulation of plant innate immunity by three proteins in a complex conserved across the plant and animal kingdoms. *Genes Dev.* **21,** 1484–1493 (2007).
8. Xu, F., Xu, S., Wiermer, M., Zhang, Y. & Li, X. The cyclin L homolog MOS12 and the MOS4-associated complex are required for the proper splicing of plant resistance genes. *Plant J.* **70,** 916–928 (2012).
9. Zhang, Y., Cheng, Y. T., Bi, D., Palma, K. & Li, X. MOS2, a protein containing G-patch and KOW motifs, is essential for innate immunity in Arabidopsis thaliana. *Curr. Biol.* **15,** 1936–1942 (2005).
10. Bi, D. *et al.* Mutations in an aypical TIR-NB-LRR-LIM resistance protein confer autoimmunity. *Front. Plant Sci.* **2,** 71 (2011).
11. D'Silva, P. R., Schilke, B., Walter, W. & Craig, E. A. Role of Pam16's degenerate J domain in protein import across the mitochondrial inner membrane. *Proc. Natl Acad. Sci. USA* **102,** 12419–12424 (2005).
12. Frazier, A. E. *et al.* Pam16 has an essential role in the mitochondrial protein import motor. *Nat. Struct. Mol. Biol.* **11,** 226–233 (2004).
13. Scheible, W. R. *et al.* An Arabidopsis mutant resistant to thaxtomin A, a cellulose synthesis inhibitor from Streptomyces species. *Plant Cell* **15,** 1781–1794 (2003).
14. Nelson, B. K., Cai, X. & Nebenfuhr, A. A multicolored set of in vivo organelle markers for co-localization studies in Arabidopsis and other plants. *Plant J.* **51,** 1126–1136 (2007).
15. Gao, M. *et al.* Regulation of cell death and innate immunity by two receptor-like kinases in Arabidopsis. *Cell Host Microbe* **6,** 34–44 (2009).
16. Greenberg, J. T., Guo, A., Klessig, D. F. & Ausubel, F. M. Programmed cell death in plants: a pathogen-triggered response activated coordinately with multiple defense functions. *Cell* **77,** 551–563 (1994).
17. Jabs, T., Dietrich, R. A. & Dangl, J. L. Initiation of runaway cell death in an Arabidopsis mutant by extracellular superoxide. *Science* **273,** 1853–1856 (1996).
18. Bowling, S. A. *et al.* A mutation in Arabidopsis that leads to constitutive expression of systemic acquired resistance. *Plant Cell* **6,** 1845–1857 (1994).
19. Maleck, K. *et al.* Isolation and characterization of broad-spectrum disease-resistant Arabidopsis mutants. *Genetics* **160,** 1661–1671 (2002).
20. Li, X., Zhang, Y., Clarke, J. D., Li, Y. & Dong, X. Identification and cloning of a negative regulator of systemic acquired resistance, SNI1, through a screen for suppressors of npr1-1. *Cell* **98,** 329–339 (1999).
21. Shah, J., Kachroo, P. & Klessig, D. F. The Arabidopsis ssi1 mutation restores pathogenesis-related gene expression in npr1 plants and renders defensin gene expression salicylic acid dependent. *Plant Cell* **11,** 191–206 (1999).
22. Gao, M. *et al.* MEKK1, MKK1/MKK2 and MPK4 function together in a mitogen-activated protein kinase cascade to regulate innate immunity in plants. *Cell. Res.* **18,** 1190–1198 (2008).
23. Yang, S. & Hua, J. A haplotype-specific Resistance gene regulated by BONZAI1 mediates temperature-dependent growth control in Arabidopsis. *Plant Cell* **16,** 1060–1071 (2004).
24. Cheng, Y. T. *et al.* Stability of plant immune-receptor resistance proteins is controlled by SKP1-CULLIN1-F-box (SCF)-mediated protein degradation. *Proc. Natl Acad. Sci. USA* **108,** 14694–14699 (2011).
25. Gou, M. *et al.* The F-box protein CPR1/CPR30 negatively regulates R protein SNC1 accumulation. *Plant J.* **69,** 411–420 (2012).
26. Miura, K. & Ohta, M. SIZ1, a small ubiquitin-related modifier ligase, controls cold signaling through regulation of salicylic acid accumulation. *J. Plant Physiol.* **167,** 555–560 (2010).
27. Miura, K., Lee, J., Miura, T. & Hasegawa, P. M. SIZ1 controls cell growth and plant development in Arabidopsis through salicylic acid. *Plant Cell Physiol.* **51,** 103–113 (2010).
28. Neupert, W. & Herrmann, J. M. Translocation of proteins into mitochondria. *Annu. Rev. Biochem.* **76,** 723–749 (2007).
29. van der Laan, M., Hutu, D. P. & Rehling, P. On the mechanism of preprotein import by the mitochondrial presequence translocase. *Biochim. Biophys. Acta* **1803,** 732–739 (2010).
30. Pais, J. E., Schilke, B. & Craig, E. A. Reevaluation of the role of the Pam18:Pam16 interaction in translocation of proteins by the mitochondrial Hsp70-based import motor. *Mol. Biol. Cell* **22,** 4740–4749 (2011).
31. Bischoff, V., Cookson, S. J., Wu, S. & Scheible, W. R. Thaxtomin A affects CESA-complex density, expression of cell wall genes, cell wall composition, and causes ectopic lignification in *Arabidopsis thaliana* seedlings. *J. Exp. Bot.* **60,** 955–965 (2009).
32. Krause, M. & Durner, J. Harpin inactivates mitochondria in Arabidopsis suspension cells. *Mol. Plant Microbe Interact.* **17,** 131–139 (2004).
33. Mehdy, M. C. Active oxygen species in plant defense against pathogens. *Plant Physiol.* **105,** 467–472 (1994).
34. Gleason, C. *et al.* Mitochondrial complex II has a key role in mitochondrial-derived reactive oxygen species influence on plant stress gene regulation and defence. *Proc. Natl Acad. Sci. USA* **108,** 10768–10773 (2011).

35. Clough, S. J. & Bent, A. F. Floral dip: a simplified method for Agrobacterium-mediated transformation of *Arabidopsis thaliana*. *Plant J.* **16,** 735–743 (1998).
36. McFarlane, H. E., Young, R. E., Wasteneys, G. O. & Samuels, A. L. Cortical microtubules mark the mucilage secretion domain of the plasma membrane in Arabidopsis seed coat cells. *Planta* **227,** 1363–1375 (2008).
37. Bindschedler, L. V. *et al.* Peroxidase-dependent apoplastic oxidative burst in Arabidopsis required for pathogen resistance. *Plant J.* **47,** 851–863 (2006).
38. Keppler, L. D., Atkinson, M. M. & Baker, C. J. Active oxygen production during a bacteria-induced hypersensitive reaction in tobacco suspension cells. *Phytopathology* **79,** 974–978 (1989).

Acknowledgements

We thank Dr Peter Rehling (University of Göttingen) for kindly giving us the *pam16-1* yeast strain, Dr Wolf-Rüdiger Scheible (MPI Golm/Potsdam) for providing seeds of *txr1-1* and Arabidopsis Biological Resource Centre (ABRC) for *Atpam16l* T-DNA insertion mutant. Dr A. Lacey Samuels is acknowledged for her insightful discussions and suggestions on the mitochondrial co-localization and cryo-immuno-TEM experiments. We are grateful for the financial support to X.L. from Natural Sciences and Engineering Research Council (NSERC) of Canada and the William Cooper Endowment Fund from U.B.C., X.C. and Y.H. are partly supported by PhD scholarships from Chinese Scholarship Council (CSC), while C.C. is partly supported by an NSERC scholarship for MSc students. CR, VL and MW acknowledge funding by the Deutsche Forschungsgemeinschaft (DFG).

Authors contributions

Y.H. and X.C. collaborated and carried out the majority of the experiments. C.R. and M.W. carried out confocal microscopy experiments. H.E.M. designed and carried out the immuno-gold labeled TEM. Y.L. made the library for whole-genome Illumina Sequencing. S.H. identified mutations in *BON1* and *SIZ1*. X.L. conceived the project and supervised the study. All authors contributed to data analysis and writing of the paper.

Additional information

Supplementary Information accompanies this paper at http://www.nature.com/naturecommunications

Competing financial interests: The authors declare no competing financial interests.

Reprints and permission information is available online at http://npg.nature.com/reprintsandpermissions/

How to cite this article: Huang, Y. *et al.* Mitochondrial AtPAM16 is required for plant survival and the negative regulation of plant immunity. *Nat. Commun.* 4:2558 doi: 10.1038/ncomms3558 (2013).